FRONTIERS OF PHYSICS

RESEARCH ARTICLE
Volume 18 / Issue 3 / 33300 / 2023

Flexible and ultrathin dopamine modified MXene and cellulose nanofiber composite films with alternating multilayer structure for superior electromagnetic interference shielding performance

Qiugang Liao[1], Hao Liu[1], Ziqiang Chen[1], Yinggan Zhang[2], Rui Xiong[1], Zhou Cui[1], Cuilian Wen[1,†], Baisheng Sa[1,‡]

1 Multiscale Computational Materials Facility, and Key Laboratory of Eco-materials Advanced Technology, College of Materials Science and Engineering, Fuzhou University, Fuzhou 350100, China
2 College of Materials, Fujian Provincial Key Laboratory of Theoretical and Computational Chemistry, Xiamen University, Xiamen 361005, China
Corresponding authors. E-mail: †clwen@fzu.edu.cn, ‡bssa@fzu.edu.cn
Received July 1, 2022; accepted November 24, 2022

ABSTRACT

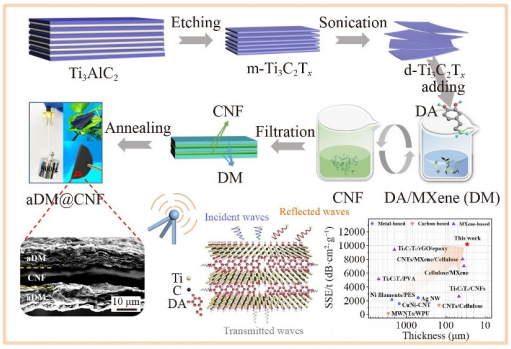

With the development of modern electronics, especially the next generation of wearable electromagnetic interference (EMI) shielding materials requires flexibility, ultrathin, lightweight and robustness to protect electronic devices from radiation pollution. In this work, the flexible and ultrathin dopamine modified MXene@cellulose nanofiber (DM@CNF) composite films with alternate multilayer structure have been developed by a facile vacuum filtration induced self-assembly approach. The multilayered DM@CNF composite films exhibit improved mechanical properties compared with the homogeneous DM/CNF film. By adjusting the layer number, the multilayered DM3@CNF2 composite film exhibits a tensile strength of 48.14 MPa and a toughness of 5.28 MJ·m^{-3} with a thickness about 19 μm. Interestingly that, the DM@CNF film with annealing treatment achieves significant improvement in conductivity (up to 17264 S·m^{-1}) and EMI properties (*SE* of 41.90 dB and SSE/t of 10169 dB·cm^2·g^{-1}), which still maintains relatively high mechanical properties. It is highlighted that the ultrathin multilayered DM@CNF film exhibits superior EMI shielding performance compared with most of the metal-based, carbon-based and MXene-based shielding materials reported in the literature. These results will offer an appealing strategy to develop the ultrathin and flexible MXene-based materials with excellent EMI shielding performance for the next generation intelligent protection devices.

Keywords MXene, dopamine, cellulose nanofibers, electromagnetic interference shielding performance, mechanical properties

1 Introduction

The booming electronic devices and wireless communication technology with enhanced signal strength and transmission rate have improved our life quality. However, it also generates severe electromagnetic interference (EMI) radiation, which significantly reduces the accuracy of electronic devices and even threatens human

*Special Topic: MXene and Its Applications (Eds.: Qing Huang, Ju Han Lee & Guangcun Shan).

https://doi.org/10.1007/s11467-022-1234-6

health [1–8]. The traditional conductive metal and metallic composites have been used to minimize the hazards of electromagnetic pollution, but their susceptibility to corrosion, unbend ability, high weight and large thickness run counter to the requirements of next-generation wearable protection devices [9–11]. Besides that, the conductive polymer-based composites (CPC) are considered as the EMI shielding materials due to their light weight, low cost and corrosion resistance [12, 13]. However, their EMI shielding effectiveness (SE) is closely related to the conductivity, which will require more conductive filler loading [14, 15]. Recently, various low dimensional carbon [16–19] and graphene-related derivatives [15, 20–22] have been designed as potential EMI shielding materials since they possess large specific surface area and good electron mobility. However, the dispersion of the aqueous solution of the carbon nanotube and graphene is poor, and the absorption effect on electromagnetic waves is limited due to the restriction of ultrathin thickness [23, 24]. Therefore, it is urgently desirable and challenging to design and explore novel flexible, lightweight and ultrathin candidates with desirable EMI shielding performance.

Since being discovered in 2011, MXene has attracted tremendous attentions in many applications, including catalysis [25], energy storage [26, 27] and [17] biomedical materials [28] due to their excellent electrochemical properties, abundant active functionalities and environmental friendliness [29–33]. Note that, MXene has been demonstrated as a potential candidate for EMI shielding application due to their 2D nanostructure, excellent electrical properties, high hydrophilicity and various surface functional groups [34–37]. The $Ti_3C_2T_x$ film with a thickness of 45 μm was reported to have a high EMI SE of 92 dB, which is most superior among the materials with similar thickness [38]. Unfortunately, the MXene-based films usually suffer from mechanical fragility due to their weak interflake interaction and bending flexibility [39], which severely limits their further EMI shielding related applications.

Generally, the polymer modified composites are considered as good candidates to be combined with the hydrophilic functional groups of MXene due to their lightweight, flexibility, and hydrophilicity, then effectively improve the mechanical properties of MXene [40, 41]. In particular, the cellulose nanofiber (CNF) is potential utilized as the reinforce matrix in layered films due to its one-dimensional structure, good mechanical properties and the hydrophilic and polyhydroxy characteristics make it suitable for the solution process [42]. Unfortunately, the combination of organic materials and MXene to improve mechanical properties usually leads to a reduction of electrical conductivity [43, 44]. It was reported that the MXene/CNF paper with 50 wt% CNF exhibit drastic deterioration in electrical conductivity only to 9.69 $S{\cdot}m^{-1}$ and EMI property to 21 dB due to the increased contact resistance [45]. Therefore, considering that MXene with rich active groups (–OH, =O, and –F) are easily oxidized [46], and the homogeneous MXene/CNF composite generally reduce the electrical conductivity, the suitable structural design of the MXene-based composite films with high mechanical properties and EMI performance are of great significance and related studies in this regard are quite limited.

On the other hand, dopamine (DA) is highly hydrophilic and adsorptive, which makes it possible to self-polymerise dopamine onto the surface of two-dimensional layered MXene to build composite films, then improve the oxidation resistance [40]. Previous work reported that dopamine can be polymerized in situ and combined with MXene flakes by spontaneous interfacial charge transfer, which further improve the mechanical properties and the innate high electrical conductivity [47]. The results indicate that the modification of dopamine could possibly enhance the antioxidant properties and hydrophilicity of MXene and play as the adhesive connection to CNF layer. Therefore, the facile fabrication of ultrathin and flexible dopamine modified MXene@cellulose nanofiber (DM@CNF) composite films, and the comprehensive understanding of the structural characterization, mechanical properties and EMI shielding functions are of great important and interest.

In this work, we have proposed the flexible and ultrathin DM@CNF composite films with alternating multilayer structure via a facile alternating vacuum filtration method. Furthermore, we have also systematically investigated the microstructures, mechanical properties and EMI shielding performance of the proposed composite film. In this multilayer structure, the flexibility, toughness, and hydrophilicity of the independent CNF buffer layer make it easy to bond with the DM layer and effectively prevent the rapid growth of cracks under external forces, providing the composite film with high mechanical properties. By adjusting the layer number, the mechanical properties and EMI performance of the multilayered DM@CNF films have been systematically evaluated. Additionally, the effect of annealing treatment on mechanical properties, electrical conductivity and EMI performance of DM@CNF composite films are also demonstrated. The multilayered DM@CNF composite films exhibit significant improvement in conductivity (up to 17264 $S{\cdot}m^{-1}$) and EMI properties (SE of 41.90 dB and SSE/t of 10169 $dB{\cdot}cm^2{\cdot}g^{-1}$). Furthermore, we have unraveled the electromagnetic shielding mechanism of multilayered DM@CNF films. Therefore, our study paves the way to provide a feasible strategy for the design of MXene-based materials with high mechanical properties and superior EMI shielding performance for the protection of electronic devices, such as wearable electronic products and smart microelectronics.

2 Experimental

2.1 Materials and chemicals

Ti_3AlC_2 (MAX, 400 mesh) powder was purchased from 11 Technology Co., Ltd., China. Dopamine hydrochloride (98%) was supplied by Macklin, Shanghai, China. Lithium fluoride (LiF, AR) was provided from Aladdin Reagent, China. Hydrochloric acid (HCl, 37–38 wt%) and ethanol absolute (EtOH) were provided by Sinopharm Chemical Reagent Co., Ltd., China. CNF aqueous solution (1 wt%) was purchased from Guilin Qihong Technology Co., Ltd., China.

2.2 Synthesis of $Ti_3C_2T_x$ MXene

The $Ti_3C_2T_x$ MXene was prepared via a modified LiF/HCl etching process [48]. Firstly, 1 g of LiF was dissolved in 20 ml of 9 M HCl solution and stirred slowly for 10 min. Then 1 g of Ti_3AlC_2 MAX powder was gradually added, and the etching process was conducted at 35 °C for 48 h to extract the Al layers. Subsequently, the suspension was washed several times with deionized water along with repeat centrifugation (4000 rpm, 10 min), until the pH value reached to 6–7. The obtained $Ti_3C_2T_x$ suspension was sonicated (500 W) in the water for another 40 min. Finally, the suspension was centrifuged at 4000 rpm for 30 min, then transferred to vacuum freeze dryer for 12 h to obtain the dried MXene powder.

2.3 Preparation of alternating multilayered DM@CNF films

The multilayered DM@CNF films were synthesized via a facile alternate vacuum filtration (AVF) induced self-assembly process. Initially, dopamine hydrochloride was added dropwise into 15 mL of $Ti_3C_2T_x$ aqueous solution by a predetermined weight ratio ($Ti_3C_2T_x$:dopamine hydrochloride were 100:6), then the aqueous solution was further stirred for 60 min to obtain DM solution. Subsequently, the continuous thin DM layer was filtered on a filter membrane. Then, 2 g of CNF (1 wt%) was added into 10 mL of an aqueous solution divided into 1 or 2 parts equally and deposited on the top of initial DM layer. After that, another part of DM layer was covered on the surface of CNF layer to form a sandwich-like structure. Finally, the resulting multilayered films were dried at ambient temperature and carefully removed from the filtration membrane. By changing the layer number, the films were alternately made into 3 and 5 layers, respectively, which are correspondingly abbreviated as DM2@CNF1 and DM3@CNF2. As a comparison, homogeneous DM/CNF films have been prepared by similar method but directly mixing same content of CNF and DM aqueous solution. The MXene, DM and DM/CNF films were also fabricated via a similar vacuum filtration process. The amounts of CNF, dopamine and MXene were kept the same in all composite films. Finally, the DM/CNF, DM2@CNF1, and DM3@CNF2 films were annealed at 150 °C for 6 h in a muffle furnace to obtain annealed films, which were denoted as aDM/CNF, aDM2@CNF1, and aDM3@CNF2, respectively.

2.4 Characterizations

The morphology and elemental distribution of samples were characterized by SEM (SUPRA-55, Zeiss) combined with energy dispersive spectrometry (EDS). The crystalline structure of samples were characterized by XRD (Miniflex 600, Rigaku) with Cu K_α radiation of $\lambda = 0.15418$ nm. FTIR spectrometry (Nicolet 5700, Thermo) was used to analyze the functional groups of samples, ranging from 500 to 4000 cm^{-1}. XPS spectroscopy (K-Alpha+, Thermo) was adopted to analyze the chemical composition of MXene. TGA analysis (STA 449-F5, Netzsch) was conducted at a stabilized flow of 20 ml/min of nitrogen from ambient temperature to 600 °C. The conductivity of the prepared samples was measured by the multifunctional digital four-probe tester (ST-2258c, Jingge Co., Ltd., China). The mechanical properties of the samples were tested using a universal tensile machine (MTS-E44, MTS Systems Co., Ltd., China) with rectangular samples of 25 mm × 10 mm and loading rate of 0.5 mm/min.

The electromagnetic parameters of composite film materials were acquired using a network analyzer (N5234A, Agilent Technologies, America) in the 8.2-12.4 GHz (X-band) frequency band at ambient temperature. Before the measurement, the specimen was cut into rectangular slices (22.58 mm × 10.14 mm × 0.04 mm). The total electromagnetic interference shielding values (SE_T) were calculated according equations as follows [49]:

$$R = |S_{11}|^2, T = |S_{21}|^2, \tag{1}$$

$$A = 1 - R - T, \tag{2}$$

$$SE_A = -10 \log \frac{T}{1-R}, SE_R = -10 \log (1-R), \tag{3}$$

$$SE_T = SE_R + SE_A + SE_M, \tag{4}$$

where S_{11} and S_{21} are scattering parameters. R, A and T are reflection, absorption and transmission coefficients, respectively. SE_R is the microwave reflection, SE_A is the microwave absorption. SE_M is the multiple reflection, which can be negligible when $SE_T \geq 15$ dB.

3 Results and discussion

The schematic illustration of the preparation process of

multilayered DM@CNF composite films is presented in Fig. 1. The $Ti_3C_2T_x$ MXene was prepared via selective etching of Al layers from Ti_3AlC_2 MAX precursor with HCl/LiF mix solution and further delaminating under ultrasonic. Then the dopamine (DA) was added into the $Ti_3C_2T_x$ MXene solution for modification to obtain DA/MXene (DM), which could possibly improve the electron transport rate and depress the thermal decomposition of $Ti_3C_2T_x$ MXene [47]. Subsequently, the multilayered DM@CNF composite films could be obtained by alternating vacuum filtration of DM and CNF solutions. Afterward, the obtained films were annealed under 150 °C for 6 h, which were denoted as aDM@CNF films. Through this strategy, the multilayer DM@CNF and aDM@CNF films are easy to be manufactured and exhibit good mechanical properties, which can hold a 500 g weight without any breaking. Moreover, the annealed aDM@CNF composite films were lightweight, flexible and can thus be folded into any shape without any damage.

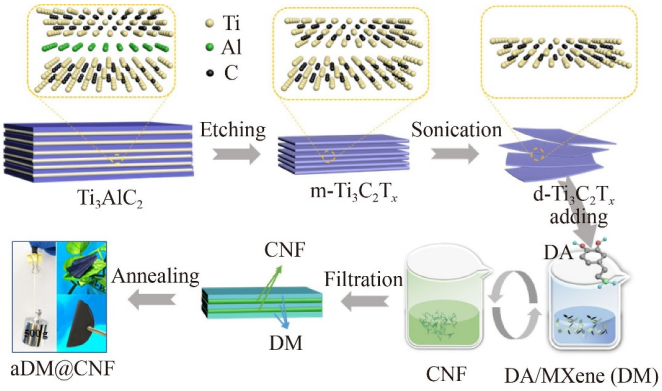

Fig. 1 Schematic illustration of the preparation process of $Ti_3C_2T_x$ nanosheets and multilayered DM@CNF composite films.

The SEM images of the Ti_3AlC_2 MAX and $Ti_3C_2T_x$ nanosheets are shown in Figs. 2(a) and (b). It is seen that the d-$Ti_3C_2T_x$ nanosheets have been etched from Ti_3AlC_2 with dense block after etching and ultrasonic process. XRD spectra were used to compare the difference of crystal structures between Ti_3AlC_2 and $Ti_3C_2T_x$, as shown in Fig. 2(c). The enhancing peak (002) crystal plane significantly shifts to the left side, indicating that the expansion of interlayer spacing due to the etching

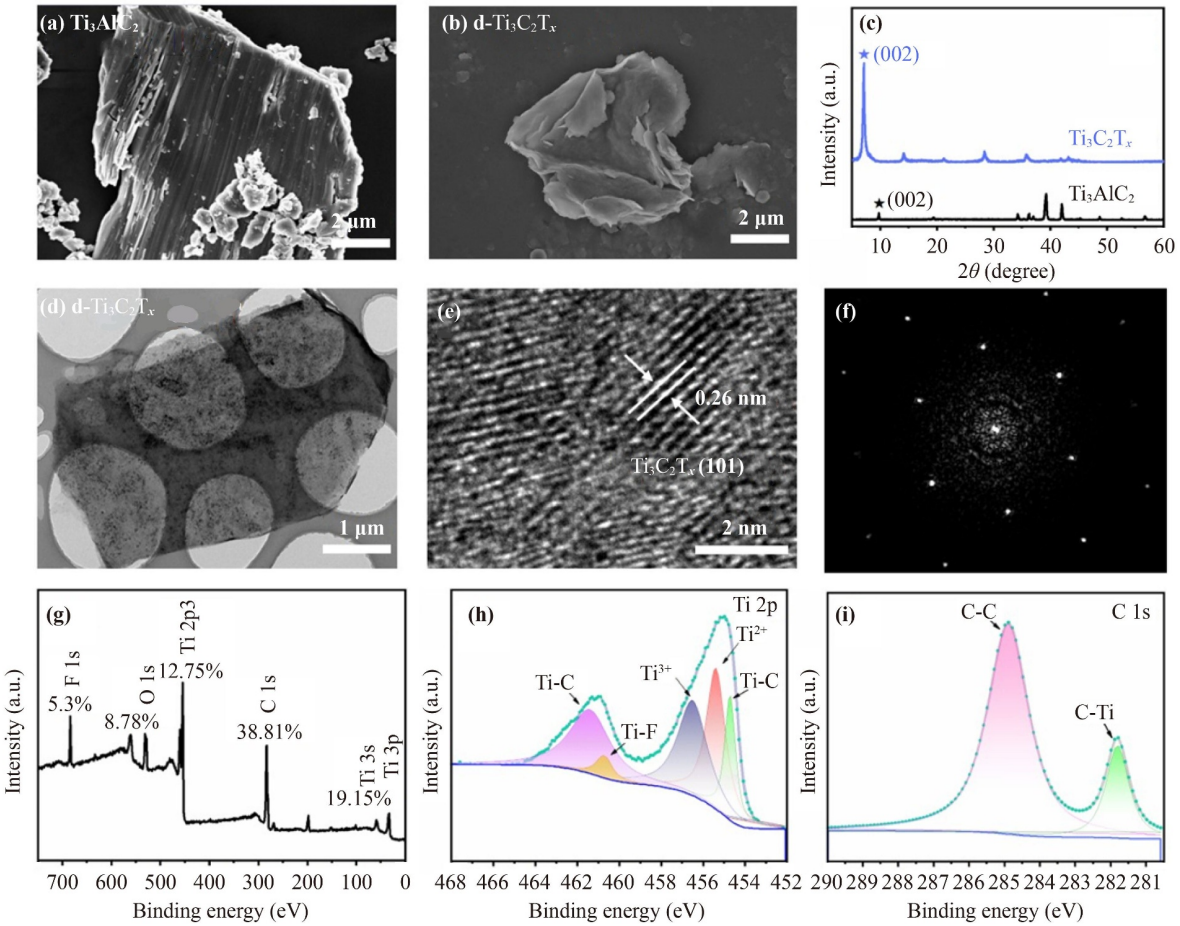

Fig. 2 The SEM images of **(a)** Ti_3AlC_2 and **(b)** d-$Ti_3C_2T_x$ nanosheets, **(c)** XRD patterns of Ti_3AlC_2 and d-$Ti_3C_2T_x$ nanosheet. **(d)** TEM, **(e)** HRTEM and **(f)** SAED images of d-$Ti_3C_2T_x$ nanosheets. **(g)** XPS survey spectra and the corresponding **(h)** Ti 2p and **(i)** C 1s spectra of d-$Ti_3C_2T_x$ nanosheets.

and exfoliation of Al layers [42]. Furthermore, the relevant TEM, HRTEM and SAED images of d-$Ti_3C_2T_x$ nanosheet are depicted in Figs. 2(d)–(f). It shows that the as-prepared d-$Ti_3C_2T_x$ nanosheet exhibits a transparent slice structure, which is confirmed by its HRTEM images. The selected area electron diffraction (SAED) in Fig. 2(f) also reveals its high-crystalline nature with a few layer structure. Moreover, XPS spectra of $Ti_3C_2T_x$ in Fig. 2(g) shows that the peaks at 453.78, 283.49, 528.19, and 683.52 eV are corresponded to Ti 2p, C 1s, O 1s, and F 1s, respectively. The absence of Al 2p peak at 74.5 eV observed in the $Ti_3C_2T_x$ sample indicates that Al layer has been chemically etched, well consisted with XRD and SEM results. Figure 2(h) exhibits the Ti 2p spectra of $Ti_3C_2T_x$, whose peaks at 455.3, 455.6, 457.5, 460.9 and 461.8 eV are attributed to Ti–C (Ti $2P_{3/2}$), Ti^{2+} (Ti $2P_{3/2}$), Ti^{3+} (Ti $2P_{3/2}$), C–Ti–F (Ti $2P_{3/2}$) and Ti–C (Ti $2P_{1/2}$), respectively. Additionally, the C 1s spectra of d-$Ti_3C_2T_x$ nanosheets display two sharp peaks at 281.9 and 284.7 eV in Fig. 2(i), which are related to the C–Ti and C–C bonds, respectively [50]. These results verify that the d-$Ti_3C_2T_x$ nanosheets have been successfully exfoliated.

Furthermore, the crystal structures of d-$Ti_3C_2T_x$ MXene film, DM, DM/CNF, DM2@CNF1 and DM3@CNF2 composite films before and after annealing have been investigated, as illustrated in Fig. 3(a). It notes that MXene film with a significant (002) diffraction peak of 7.0° has been shifted to 6.8° for DM films. This indicates that the increase of layer spacing caused by the addition of dopamine into the MXene, which can adhere to the surface of d-$Ti_3C_2T_x$ nanosheets for its strong adsorption [47]. The DM/CNF, DM2@CNF1 and DM3@CNF2 composite films exhibits similar characteristic (002) peak of DM film. By contrast, the films after annealing (aDM/CNF, aDM2@CNF1 and aDM3@CNF2) can result in the (002) diffraction peak further shifting into the left side. It implies that annealing treatment can further increase the crystal plane spacing of the composite film, which could be due to volatilization of water and the thermal decomposition of CNF. The FTIR spectra of the CNF, $Ti_3C_2T_x$ MXene, DM/CNF and DM2@CNF1 composite films are displayed in Fig. 3(b). There are two typical peaks of $Ti_3C_2T_x$ at 1390 and 551 cm^{-1}, which are corresponded to the surface end groups of C–F and –OH, respectively. The characteristic absorption bands of cellulose with the 2911 cm^{-1} (C–H stretching), 1604 cm^{-1} (–OH bending), and 619 cm^{-1} (OH bending), are observed in DM/CNF and DM2@CNF1 composite films [49]. Meanwhile, for the functionalization of dopamine, the characteristic absorption band broadens at 3000–3700 cm^{-1} could be attributed to the simultaneous action of –OH and $–NH_2$ stretching vibrations [51]. Furthermore, TGA analyses has been performed to study the decomposition and thermal stability of the samples, as depicted in Fig. 3(c).

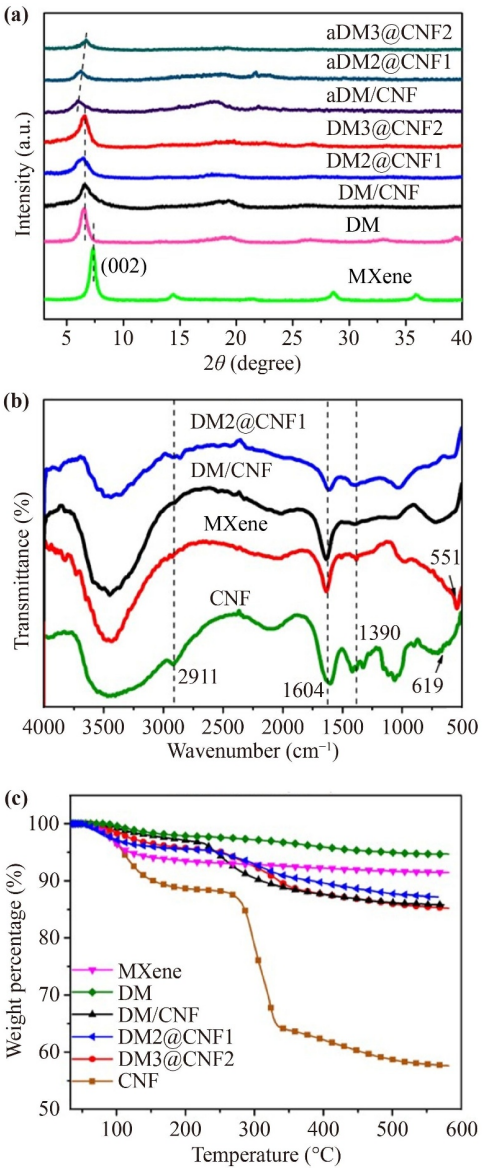

Fig. 3 **(a)** XRD patterns of the d-$Ti_3C_2T_x$ MXene, DM composite, DM/CNF, DM2@CNF1 and DM3@CNF2 composite films before and after annealing. **(b)** FTIR spectra of the CNF, d-$Ti_3C_2T_x$ MXene, DM/CNF and DM2@CNF1 composite films. **(c)** TG curves of the CNF, d-$Ti_3C_2T_x$ MXene, DM, DM/CNF, DM2@CNF1 and DM3@CNF2 composite films.

It is clear that pure CNF has the largest weight loss ratio, which is mainly reflected in two mass loss processes. The first mass loss occurs around 100–150 °C with a weight loss of approximately 5% due to the volatilization of water. The second mass loss emerges in a weight loss of approximately 25% near 270–330 °C attributed to the thermal decomposition of CNF. It is worth noting that the mass loss of DM is significantly less compared with that of $Ti_3C_2T_x$ MXene at the whole stage, indicating that DM has a resistance to thermal decomposition and oxidation resistance at high temperatures [47]. The result also implies that that the multilayered

DM@CNF composite films with dopamine modification can ensure themselves not be destroyed during the annealing process. For multilayered DM2@CNF1 and DM3@CNF2 composite films, the first mass loss occurs around 100 °C with approximately 3% mass loss for the volatilization of water and the second event emerges about 5% weight loss near 300 °C ascribed to the CNF thermal decomposition.

The cross-sectional SEM images of homogeneous DM/CNF, multilayered DM2@CNF1, aDM2@CNF1 and DM3@CNF2 composite films are displayed in Fig. 4. It observes that the DM/CNF film exhibits uniform well alignment distribution, without any obvious dislocation and peeling. Interestingly, it is noted that one CNF layer with a thickness about 10 μm is sandwiched between two DM layers with highly ordered alternating lamellar structures along the in-plane direction for DM2@CNF1 composite films [Fig. 4(b)], which is quite different from the DM/CNF film. Compared with DM2@CNF1 film, the lamellar structure of aDM2@CNF1 film increases after annealing treatment, indicating that the evaporation of water and the thermal decomposition of CNF caused by annealing can enlarge the spacing between the lamellas. Moreover, the DM3@CNF2 film displays obvious three DM layers respectively wrap with two CNF layers, as shown in Fig. 4(d). The corresponding Ti, C, and N elemental surface distribution mappings of DM3@CNF2 film reveal that the homogenous distributions without distinctive local agglomerations. The highly ordered alternating lamellar structures of multilayer DM@CNF films can offer the possibility of achieving enhancing electromagnetic shielding due to reflection-absorption-zigzag reflection mechanism [49]. Therefore, the multilayered DM@CNF structure films could be not only favorable for the mechanical properties but are also beneficial to the electromagnetic shielding performance.

Mechanical properties are essential for materials practically applied in electromagnetic shielding. Figure 5(a) shows the typical stress-strain curves of the pristine MXene, CNF, DM films and different DM/CNF, DM2@CNF1 and DM3@CNF2 composite films before and after annealing treatment. The corresponding tensile strength and toughness are displayed in Fig. 5(b). The MXene shows relatively poor tensile properties due to the weak intermolecular force and hydrogen bonding maintaining strength [39]. The pure CNF exhibits a fracture strain of 16.5% and a toughness of 1.4 MJ·m^{-3}, which can be utilized to enhance MXene interactions and facilitate stress transfer, thereby improving mechanical properties. Thus, the DM/CNF, DM2@CNF1 and DM3@CNF2 composite films display significantly better tensile strength than MXene and DM films. Among them, it is worth noting that the multilayered DM3@CNF2 composite films exhibit strongest ultimate tensile strength and toughness up to 48.14 MPa and 5.28 MJ·m^{-3}. The result illustrates that the toughness can be dramatically enhanced by the design of multilayer structures. This multilayered structure can give free rein the mechanical properties of CNF layer. Additionally, the multilayer aDM3@CNF2 composite film retain relatively high tensile strength and toughness after annealing.

The cross-sectional SEM images of the fracture surfaces are employed to confirm the fracture mechanism of composite films, as shown in Figs. 5(c) and (d). It observes that the relatively uniform fracture surface formed and the cracks extend rapidly for homogeneous DM/CNF film since there is no intact CNF layer as a

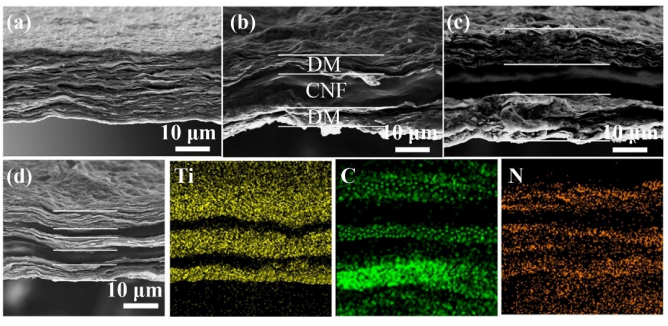

Fig. 4 The cross-sectional SEM images of **(a)** DM/CNF, **(b)** DM2@CNF1, **(c)** aDM2@CNF1 composite films, and **(d)** the cross-sectional SEM morphology and elemental mapping images of DM3@CNF2 composite film.

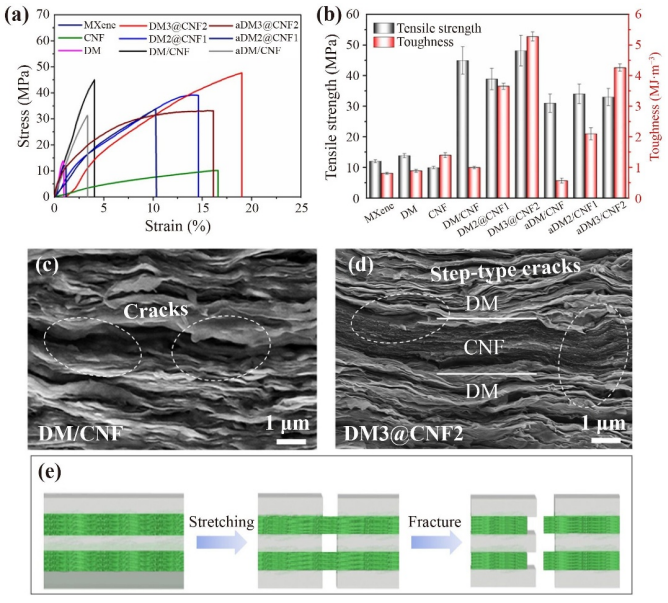

Fig. 5 **(a)** The tensile stress-strain curves and **(b)** tensile strength and toughness of the $Ti_3C_2T_x$ MXene, CNF films, DM composite, DM/CNF, DM2@CNF1 and DM3@CNF2 composite films before and after annealing, the cross-sectional SEM micrographs of the fracture surfaces of the **(c)** DM/CNF and **(d)** DM3@CNF2 films, and **(e)** the schematic illustration of the fracture mechanism of the multilayered DM3@CNF2 film.

buffer layer. On the contrary, the multilayered DM3@CNF2 composite film exhibits a typical "zigzag" fracture surface with extended DM layers compared with homogeneous DM/CNF film. In addition, step-type cracks can be obviously observed on the fracture surface of the DM3@CNF2 film, which is mainly attributed to the hydrogen bonding interaction between CNF and DM, as well as the excellent toughness of the CNF layer. Hence, the fracture surface of the multilayered DM3@CNF2 film reveals a layered step morphology in which micron-scale step-shaped cracks observed between the layers. Such multilayer structure can absorb a large amount of fracture energy during crack extension, thus significantly enhancing the tensile strength and toughness [52]. To understand the reinforced toughening mechanism of multilayered DM3@CNF2 structure, a fracture model is proposed as illustrated in Fig. 5(e). For alternating multilayered DM3@CNF2 composite film, the DM layers are the first to be broken due to its relative rigidity with increasing stress and strain. And fortunately, the flexible CNF layers relied on the hydrogen bonding between the layers can effectively relieve the stress concentration and stop the cracks expansion. The CNF layers here act as a buffer layers to keep the whole structure from fracture until the CNF is completely damaged at stronger stress and strain. Compared with homogeneous DM/CNF film, the alternating multilayered DM3@CNF2 film needs more stress and energy to break, and a micron-scale stepped crack path of CNF layer can be formed between two DM layers at the same time, which exhibits superior mechanical properties [49].

Furthermore, the electrical conductivity of materials has a significant impact on electromagnetic shielding, which can relatively reflect the EMI shielding effectiveness (SE) [53]. Hence, the electrical conductivity and the digital images of LED light of MXene, DM, DM/CNF, DM2@CNF1 and DM3@CNF2 films before and after annealing process have been investigated, as depicted in Figs. 6(a) and (b). It shows that the freestanding MXene film displays a considerably high conductivity of 10690 $S \cdot m^{-1}$ with superior electron transport capability. After the dopamine introduced into MXene, the conductivity of DM increases to 12138 $S \cdot m^{-1}$. It is noteworthy that the conductivity of MXene and DM films after annealing are more than twice of the films before annealing, and the conductivity of DM film after annealing can even reach up to 35200 $S \cdot m^{-1}$. The improvement of electrical conductivity in MXene and DM films is attributable to the fact that annealing treatment changes the microscopic morphology of the films due to the evaporation of water, resulting in more connected layers, thus significantly improving electron transport efficiency [46, 54]. In addition, the conductivity of the homogeneous DM/CNF film is 899 $S \cdot m^{-1}$, while the conductivity of multilayered DM2@CNF1 composite film increases to 5498 $S \cdot m^{-1}$ due to the continuous conductive layer of DM on the outer

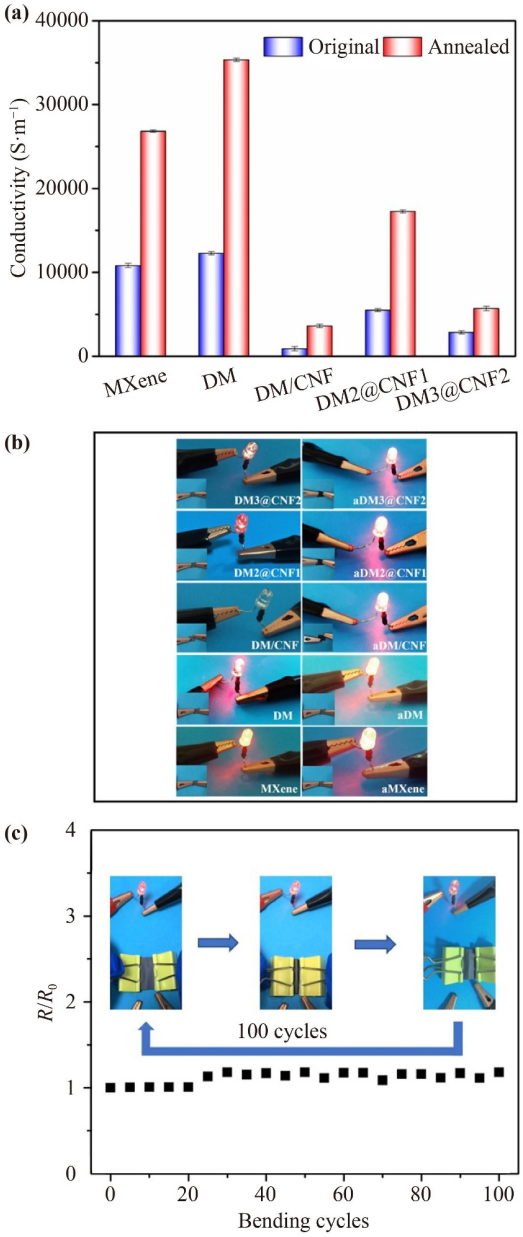

Fig. 6 **(a)** The electrical conductivity and **(b)** the digital images of LED light of $Ti_3C_2T_x$ MXene, DM, DM/CNF, DM2@CNF1 and DM3@CNF2 films before and after annealing, and **(c)** the electrical resistance variation of aDM3@CNF2 composite film with a bending test.

surface of the film. Compared with the homogeneous DM/CNF film, the multilayered DM@CNF composite films exhibit enhanced electrical conductivity, in particularly, aDM2@CNF1 possess an excellent electrical conductivity up to 17264 $S \cdot m^{-1}$. It is worth noting that the conductivity of as-prepared MXene, DM, DM/CNF, DM2@CNF1 and DM3@CNF2 films all increase remarkably after annealing treatment, which can be evidently reflected by the brightness variation of the LED bulbs in Fig. 6(b). Moreover, it have to be mentioned that the annealing treatment does not significantly reduce the

mechanical strength of the composite film, which can be ascribed to the fact that the CNF layer structure is not damaged under the annealing process of 150 °C.

In order to evaluate the conductivity stability of the composite film under external force, the electrical resistance variation of aDM3@CNF2 composite film with a bending test for 100 cycles has been further investigated, as illustrated in Fig. 6(c). The aDM3@CNF2 composite film was fixed between two insulating clips and connected to a small LED bulb with two thin copper wires to study the change of resistance during bending. It notes that the composite film exhibits no significant increase in resistance even after 100 bending cycles and the LED bulbs always maintains a stable brightness (Movie S1). The detailed electrical resistance data of aDM3@CNF2 composite film under bending test have also been listed in Table S1 of Supporting Information. The excellent flexibility and stable conductivity indicate that this multilayer composite film has tremendous potential for application in wearable electronic flexible devices.

MXene has been manifested to possess excellent EMI shielding effectiveness due to its rich charge carriers, laminated structures and surface functionalities [36]. Herein, we explore the EMI shielding performances of DM@CNF composite films to manifests their practical applications such as smart microelectronics devices. The total EMI shielding effectiveness of the DM/CNF, DM2@CNF1 and DM3@CNF2 composite films before and after annealing are plotted in Figs. 7(a) and (b). Overall, the total EMI SE of all composite films exhibit relatively stable fluctuation throughout the X-band. It observes that homogeneous DM/CNF film displays lowest EMI SE value about 14 dB, which cannot satisfy the industrial requirements for EMI materials. Interestingly that, the EMI SE of homogeneous DM/CNF film after annealing (aDM/CNF film) can reach to about 30 dB. It is highlighted that the multilayered DM2@CNF1 and DM3@CNF2 composite films before and after annealing all exhibit relatively high EMI SE > 30 dB, and the EMI SE increases significantly with the increase of conductivity of the films, which meets the requirements of most industrial applications. Significantly, the EMI SE of DM3@CNF2 film is about 38.5 dB, which is higher than that of DM2@CNF1 (30.2 dB). As the number of DM and CNF layers increases from 3 to 5, the multiple reflections of EMI can be enhanced, leading to higher EMI SE (30.1 Vs 38.5 dB). In addition, the EMI SE of the multilayered aDM2@CNF1 composite films is 41.9 dB, which is superior to DM1@CN2 film (30.1 dB). Furthermore, the EMI SE of aDM3@CNF2 film increases slightly compared with that before annealing, which is well consistent with the variation of conductivity. It should be pointed out that the influence of the layer design on the conductivity of the samples will be reduced after annealing treatment. This can be explained by that evaporation of water and

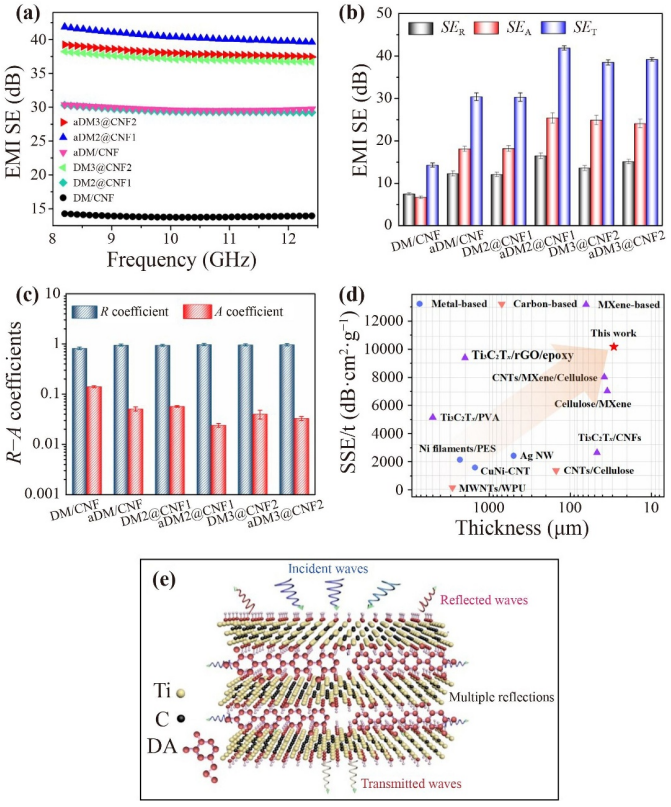

Fig. 7 **(a)** The EMI shielding performance, **(b)** the average EMI shielding effectiveness (SE_T), microwave absorption (SE_A) and microwave reflection (SE_R) values, and **(c)** the R–A coefficients of DM/CNF, DM2@CNF1 and DM3@CNF2 composite films before and after annealing. **(d)** The SSE/t as a function of thickness compared with previous reports, and **(e)** schematic illustration of the electromagnetic wave transfer across the multilayered DM@CNF composite films.

the diffusion of the interface between DM and CNF layer under annealing process could enhance the good connectivity of MXene and further enhance the electric conductivity. As a result, the EMI SE values of aDM2@CNF1 and aDM3@CNF2 films with annealed treatment are quite similar, which is about 41.9 and 38.5 dB, respectively. The results also indicate that the excellent conductivity of the multilayered DM@CNF composite films can be beneficial for the superior EMI performance.

To further understand the EMI shielding mechanism, and the average EMI shielding effectiveness (SE_T), microwave absorption (SE_A) and microwave reflection (SE_R) values of DM/CNF, DM2@CNF1 and DM3@CNF2 composite films before and after annealing were calculated based on Eqs. (3) and (4), as depicted in Fig. 7(b). It finds that homogeneous DM/CNF film is inferior to the multilayered DM2@CNF1 and DM3@CNF2 composite films both in reflecting and absorbing electromagnetic waves. There is no much difference in reflecting electromagnetic waves by comparing DM2@CNF1 with DM3@CNF2 films.

However, it is worth noting that DM3@CNF2 film exhibits better performance in absorbing electromagnetic waves, which contributes its optimal value of SE_T. Surprisingly, the SE_R shows an opposite change tendency with the conductivity of multilayered DM@CNF films. It seems to contradict the impedance mismatch theory, which states that the electromagnetic shielding increases with increasing impedance mismatch [35]. However, the multilayer structure of composite films can lead to a stepped reflection-absorption mechanism for EMI performance, which can counteract the reduction of the impedance mismatch effect. Compared the EMI SE value of DM2@CNF1 and DM3@CNF2 films, the influence of the multiple stepped reflection-absorption mechanism becomes more significantly as the number of multilayers increase from 3 to 5, leading the increasing SE_A value of DM3@CNF2 films. It is worth noting that the composite films after annealing have better SE_T than those before annealing, especially for aDM2@CNF1 film. In general, EM waves would be firstly reflected due to the impedance mismatch when hitting EM materials. Consequently, the SE_R value more than 10 dB signifies more than 90% of the EM waves can be reflected before entering the films [49]. Furthermore, the EMI coefficients calculated according to Eqs. (1) and (2) describe the reflection coefficient of $R > 0.9$ and the absorption coefficient of $A < 0.1$ as plotted in Fig. 7(c), indicating an absorption-reflection but reflection-dominated shielding mechanism [55]. Compared with homogeneous DM/CNF film, the multilayered DM@CNF films shows higher reflection coefficient due to its sharp increase in conductivity and stepped reflection-absorption mechanism. Moreover, the reflection coefficient of multilayered DM@CNF films can be further improved after annealing, thus enhancing the electromagnetic shielding performance.

Currently, metal-based [56] and carbon-based [57] materials are the dominant electromagnetic shielding materials with some respective advantages. Nevertheless, few materials with simultaneous ultrathin thickness, flexibility, and excellent EMI shielding performance have been reported. To further fairly evaluate the EMI shielding performance of the multilayered DM@CNF composite films, the specific SSE/t value (SE value divided by the density and thickness of composite films) [45] was calculated. The SSE/t value of the designed aDM2@CNF1 films with a thickness of 0.029 mm can reach up to 10169 $dB \cdot cm^2 \cdot g^{-1}$, which is ascribed to its multilayer structure, the reduced density and improved electrical conductivity after annealing process. It is noteworthy that the ultrathin multilayered aDM2@CNF1 film exhibits more superior EMI shielding performance compared with most of the metal-based, carbon-based and MXene-based shielding materials reported in the literatures [Fig. 7(d), Table S2 of Supporting information].

The electromagnetic shielding mechanism of multilayered DM@CNF films is illustrated in Fig. 7(e). Generally, when the incident EM waves reach the surface of the multilayered DM@CNF composite film, there has three basic consumption. Firstly, Due to the impedance mismatch, some incident waves are immediately reflected at the interface of DM and air layers, which is mainly ascribed to the presence of large free electrons on the surface of DM nanosheets. In addition, when electromagnetic waves are transmitted from the first DM layer, the second DM layer, which acts as the next blocking layer, will reflect the transmitted electromagnetic waves again due to the high impedance mismatch between the CNF and the DM layer [58]. Secondly, the DM layer along the planar direction allows for a tight continuous conductive path, which imparts high conductivity to the DM layer, causing polarization loss and attenuating the energy of electromagnetic waves [49]. In addition, MXenes etched from Ti_3AlC_2 with a fluoride salt solution have strong surface activity and are prone to forming various functional groups (–OH, =O, and –F) in aqueous solutions. In particular, when subjected to alternating electromagnetic fields, local dipoles will be generated between Ti and these highly electronegative functional groups, resulting in polarization loss of electromagnetic waves [59]. Thirdly, due to the porous layered structure formed after annealing, electromagnetic waves have an "absorption-reflection-reabsorption" process in the DM layers, and this unique structure greatly enhances the shielding effect of electromagnetic waves. Moreover, the multilayer structure can enable the DM layer to act as a multi-level shield, which allows waves to be reflected back and forth between adjacent DM nanosheets until they are completely absorbed [60].

4 Conclusion

In summary, the ultrathin and flexible DM@CNF composite films with alternating multilayer structure have been successfully prepared by an alternating vacuum filtration method. Compared with homogeneous DM/CNF film, the multilayered DM@CNF composite films exhibit improved mechanical strength and toughness. By adjusting the layer number, the alternating multilayered DM3@CNF2 composite film exhibits a tensile strength of 48.14 MPa and a toughness of 5.28 $MJ \cdot m^{-3}$ with a thickness of about 19 μm. Moreover, the multilayered DM3@CNF2 composite film exhibits has high electrical conductivity (up to 2845 $S \cdot m^{-1}$) and excellent EMI SE (up to 38.50 dB). It is highlighted that the electrical conductivity of aDM2@CNF1 film can reach up to 17264 $S \cdot m^{-1}$, and the EMI SE increases from 30.30 dB to 41.90 dB after annealing treatment. Furthermore, the corresponding electromagnetic shielding SSE/t value of aDM2@CNF1 composite film is up to

10169 $dB \cdot cm^2 \cdot g^{-1}$. More importantly, the as-prepared multilayered aDM2@CNF1 film exhibits superior EMI shielding performance compared with most of the metal-based, carbon-based and MXene-based shielding materials reported in the literatures. This work provides a feasible strategy to prepare ultrathin, flexible DM@CNF composite films with high mechanical properties and superior EMI shielding performance for related electronic field, such as wearable electronic products and smart microelectronics.

Electronic supplementary material Supplementary materials are available in the online version of this article at https://doi.org/10.1007/s11467-022-1234-6 and https://journal.hep.com.cn/fop/EN/10.1007/s11467-022-1234-6 and are accessible for authorized users.

Conflicts of interest The authors declare no competing financial interest.

Acknowledgements This work was supported by the National Key Research and Development Program of China (No. 2022YFB3807200), the National Natural Science Foundation of China (Nos. 52201022 and 21973012), the Natural Science Foundation of Fujian Province (Nos. 2020J01474, 2021J06011, and 2020J01351), and the "Qishan Scholar" Scientific Research Startup Project of Fuzhou University.

References

1. F. Shahzad, A. Iqbal, H. Kim, and C. M. Koo, 2D transition metal carbides (MXenes): Applications as an electrically conducting material, *Adv. Mater.* 32(51), 2002159 (2020)
2. D. W. Jiang, V. Murugadoss, Y. Wang, J. Lin, T. Ding, Z. C. Wang, Q. Shao, C. Wang, H. Liu, N. Lu, R. B. Wei, A. Subramania, and Z. H. Guo, Electromagnetic interference shielding polymers and nanocomposites - A review, *Polym. Rev. (Phila. Pa.)* 59(2), 280 (2019)
3. C. Xiang, R. H. Guo, S. J. Lin, S. X. Jiang, J. W. Lan, C. Wang, C. Cui, H. Y. Xiao, and Y. Zhang, Lightweight and ultrathin TiO_2-$Ti_3C_2T_x$/graphene film with electromagnetic interference shielding, *Chem. Eng. J.* 360, 1158 (2019)
4. R. T. Liu, M. Miao, Y. H. Li, J. F. Zhang, S. M. Cao, and X. Feng, Ultrathin biomimetic polymeric $Ti_3C_2T_x$ MXene composite films for electromagnetic interference shielding, *ACS Appl. Mater. Interfaces* 10(51), 44787 (2018)
5. H. Abbasi, M. Antunes, and J. I. Velasco, Recent advances in carbon-based polymer nanocomposites for electromagnetic interference shielding, *Prog. Mater. Sci.* 103, 319 (2019)
6. M. Hu, N. Zhang, G. Shan, J. Gao, J. Liu, and R. K. Y. Li, Two-dimensional materials: Emerging toolkit for construction of ultrathin high-efficiency microwave shield and absorber, *Front. Phys.* 13(4), 138113 (2018)
7. X. Li, G. C. Shan, R. G. Ma, C. H. Shek, H. B. Zhao, and S. Ramakrishna, Bioinspired mineral MXene hydrogels for tensile strain sensing and radionuclide adsorption applications, *Front. Phys.* 17(6), 63501 (2022)
8. B. Liu, L. Y. Qian, Y. L. Zhao, Y. W. Zhang, F. Liu, Y. Zhang, Y. Q. Xie, and W. Z. Shi, A polarization-sensitive, self-powered, broadband and fast $Ti_3C_2T_x$ MXene photodetector from visible to near-infrared driven by photogalvanic effects, *Front. Phys.* 17(5), 53501 (2022)
9. B. Wen, M. S. Cao, M. M. Lu, W. Q. Cao, H. L. Shi, J. Liu, X. X. Wang, H. B. Jin, X. Y. Fang, W. Z. Wang, and J. Yuan, Reduced graphene oxides: Light-weight and high-efficiency electromagnetic interference shielding at elevated temperatures, *Adv. Mater.* 26(21), 3484 (2014)
10. B. Shen, W. T. Zhai, and W. G. Zheng, Ultrathin flexible graphene film: An excellent thermal conducting material with efficient EMI shielding, *Adv. Funct. Mater.* 24(28), 4542 (2014)
11. Y. Han, H. Zhong, N. Liu, Y. X. Liu, J. Lin, and P. Jin, In situ surface oxidized copper mesh electrodes for high-performance transparent electrical heating and electromagnetic interference shielding, *Adv. Electron. Mater.* 4(11), 1800156 (2018)
12. Y. Z. Feng, B. Wang, X. W. Li, Y. S. Ye, J. M. Ma, C. T. Liu, X. P. Zhou, and X. L. Xie, Enhancing thermal oxidation and fire resistance of reduced graphene oxide by phosphorus and nitrogen co-doping: Mechanism and kinetic analysis, *Carbon* 146, 650 (2019)
13. Y. Z. Feng, G. J. Han, B. Wang, X. P. Zhou, J. M. Ma, Y. S. Ye, C. T. Liu, and X. L. Xie, Multiple synergistic effects of graphene-based hybrid and hexagonal born nitride in enhancing thermal conductivity and flame retardancy of epoxy, *Chem. Eng. J.* 379, 122402 (2020)
14. X. F. Meng, D. H. Li, X. Q. Shen, and W. Liu, Preparation and magnetic properties of nano-Ni coated cenosphere composites, *Appl. Surf. Sci.* 256(12), 3753 (2010)
15. W. L. Song, X. T. Guan, L. Z. Fan, W. Q. Cao, C. Y. Wang, Q. L. Zhao, and M. S. Cao, Magnetic and conductive graphene papers toward thin layers of effective electromagnetic shielding, *J. Mater. Chem. A* 3(5), 2097 (2015)
16. K. S. Novoselov, D. V. Andreeva, W. C. Ren, and G. C. Shan, Graphene and other two-dimensional materials, *Front. Phys.* 14(1), 13301 (2019)
17. Y. C. Wang, L. H. Yao, Q. Zheng, and M. S. Cao, Graphene-wrapped multiloculated nickel ferrite: A highly efficient electromagnetic attenuation material for microwave absorbing and green shielding, *Nano Res.* 15(7), 6751 (2022)
18. M. S. Cao, W. L. Song, Z. L. Hou, B. Wen, and J. Yuan, The effects of temperature and frequency on the dielectric properties, electromagnetic interference shielding and microwave-absorption of short carbon fiber/silica composites, *Carbon* 48(3), 788 (2010)
19. L. H. Yao, W. Q. Cao, J. G. Zhao, Q. Zheng, Y. C. Wang, S. Jiang, Q. L. Pan, J. Song, Y. Q. Zhu, and M. S. Cao, Regulating bifunctional flower-like $NiFe_2O_4$/graphene for green EMI shielding and lithium ion storage, *J. Mater. Sci. Technol.* 127, 48 (2022)
20. L. C. Jia, G. Q. Zhang, L. Xu, W. J. Sun, G. J. Zhong, J. Lei, D. X. Yan, and Z. M. Li, Robustly superhydrophobic conductive textile for efficient electromagnetic interference shielding, *ACS Appl. Mater. Interfaces* 11(1), 1680

(2019)
21. L. C. Jia, C. G. Zhou, W. J. Sun, L. Xu, D. X. Yan, and Z. M. Li, Water-based conductive ink for highly efficient electromagnetic interference shielding coating, *Chem. Eng. J.* 384, 123368 (2020)
22. L. C. Jia, K. Q. Ding, R. J. Ma, H. L. Wang, W. J. Sun, D. X. Yan, B. Li, and Z. M. Li, Highly conductive and machine-washable textiles for efficient electromagnetic interference shielding, *Adv. Mater. Technol.* 4(2), 1800503 (2019)
23. G. M. Weng, J. Y. Li, M. Alhabeb, C. Karpovich, H. Wang, J. Lipton, K. Maleski, J. Kong, E. Shaulsky, M. Elimelech, Y. Gogotsi, and A. D. Taylor, Layer-by-layer assembly of cross-functional semi-transparent MXene-carbon nanotubes composite films for next-generation electromagnetic interference shielding, *Adv. Funct. Mater.* 28(44), 1803360 (2018)
24. M. Crespo, M. González, A. L. Elías, L. Pulickal Rajukumar, J. Baselga, M. Terrones, and J. Pozuelo, Ultra-light carbon nanotube sponge as an efficient electromagnetic shielding material in the GHz range, *Phys. Status Solidi Rapid Res. Lett.* 8(8), 698 (2014)
25. Z. Li, L. Yu, C. Milligan, T. Ma, L. Zhou, Y. R. Cui, Z. Y. Qi, N. Libretto, B. Xu, J. W. Luo, E. Z. Shi, Z. W. Wu, H. L. Xin, W. N. Delgass, J. T. Miller, and Y. Wu, Two-dimensional transition metal carbides as supports for tuning the chemistry of catalytic nanoparticles, *Nat. Commun.* 9(1), 5258 (2018)
26. M. R. Lukatskaya, S. Kota, Z. F. Lin, M. Q. Zhao, N. Shpigel, M. D. Levi, J. Halim, P. L. Taberna, M. Barsoum, P. Simon, and Y. Gogotsi, Ultra-high-rate pseudocapacitive energy storage in two-dimensional transition metal carbides, *Nat. Energy* 2(8), 17105 (2017)
27. B. Anasori, M. R. Lukatskaya, and Y. Gogotsi, 2D metal carbides and nitrides (MXenes) for energy storage, *Nat. Rev. Mater.* 2(2), 16098 (2017)
28. H. Lin, Y. Chen, and J. L. Shi, Insights into 2D MXenes for versatile biomedical applications: Current advances and challenges ahead, *Adv. Sci. (Weinh.)* 5(10), 1800518 (2018)
29. M. Carey and M. W. Barsoum, MXene polymer nanocomposites: A review, *Mater. Today Adv.* 9, 100120 (2021)
30. J. Z. Zhang, N. Kong, S. Uzun, A. Levitt, S. Seyedin, P. A. Lynch, S. Qin, M. K. Han, W. R. Yang, J. Q. Liu, X. G. Wang, Y. Gogotsi, and J. M. Razal, Scalable manufacturing of free-standing, strong $Ti_3C_2T_x$ MXene films with outstanding conductivity, *Adv. Mater.* 32(23), 2001093 (2020)
31. M. Naguib, O. Mashtalir, J. Carle, V. Presser, J. Lu, L. Hultman, Y. Gogotsi, and M. W. Barsoum, Two-dimensional transition metal carbides, *ACS Nano* 6(2), 1322 (2012)
32. C. Zhan, M. Naguib, M. Lukatskaya, P. R. C. Kent, Y. Gogotsi, and D. E. Jiang, Understanding the MXene pseudocapacitance, *J. Phys. Chem. Lett.* 9(6), 1223 (2018)
33. J. C. Lei, X. Zhang, and Z. Zhou, Recent advances in MXene: Preparation, properties, and applications, *Front. Phys.* 10(3), 276 (2015)
34. J. Liu, H. B. Zhang, R. H. Sun, Y. F. Liu, Z. S. Liu, A. G. Zhou, and Z. Z. Yu, Hydrophobic, flexible, and lightweight MXene Foams for high-performance electromagnetic-interference shielding, *Adv. Mater.* 29(38), 1702367 (2017)
35. Z. L. Ma, S. L. Kang, J. Z. Ma, L. Shao, Y. L. Zhang, C. Liu, A. J. Wei, X. L. Xiang, L. F. Wei, and J. W. Gu, Ultraflexible and mechanically strong double-layered aramid nanofiber-$Ti_3C_2T_x$ MXene/silver nanowire nanocomposite papers for high-performance electromagnetic interference shielding, *ACS Nano* 14(7), 8368 (2020)
36. F. Shahzad, M. Alhabeb, C. B. Hatter, B. Anasori, S. Man Hong, C. M. Koo, and Y. Gogotsi, Electromagnetic interference shielding with 2D transition metal carbides (MXenes), *Science* 353(6304), 1137 (2016)
37. O. Mashtalir, M. Naguib, V. N. Mochalin, Y. Dall' Agnese, M. Heon, M. W. Barsoum, and Y. Gogotsi, Intercalation and delamination of layered carbides and carbonitrides, *Nat. Commun.* 4(1), 1716 (2013)
38. B. Akuzum, K. Maleski, B. Anasori, P. Lelyukh, N. J. Alvarez, E. C. Kumbur, and Y. Gogotsi, Rheological characteristics of 2D titanium carbide (MXene) dispersions: A guide for processing MXenes, *ACS Nano* 12(3), 2685 (2018)
39. Y. J. Wan, X. M. Li, P. L. Zhu, R. Sun, C. P. Wong, and W. H. Liao, Lightweight, flexible MXene/polymer film with simultaneously excellent mechanical property and high-performance electromagnetic interference shielding, *Compos. Part A Appl. Sci. Manuf.* 130, 105764 (2020)
40. H. Z. Huang, X. F. Sha, Y. Cui, S. Y. Sun, H. Y. Huang, Z. Y. He, M. Y. Liu, N. G. Zhou, X. Y. Zhang, and Y. Wei, Highly efficient removal of iodine ions using MXene-PDA-Ag_2O_x composites synthesized by mussel-inspired chemistry, *J. Colloid Interface Sci.* 567, 190 (2020)
41. L. Y. Yang, J. Cui, L. Zhang, X. R. Xu, X. Chen, and D. P. Sun, A moisture-driven actuator based on polydopamine-modified MXene/bacterial cellulose nanofiber composite film, *Adv. Funct. Mater.* 31(27), 2101378 (2021)
42. W. T. Cao, C. Ma, S. Tan, M. G. Ma, P. B. Wan, and F. Chen, Ultrathin and flexible CNTs/MXene/cellulose nanofibrils composite paper for electromagnetic interference shielding, *Nano-Micro Lett.* 11(1), 72 (2019)
43. J. H. Chen, J. K. Xu, K. Wang, X. R. Qian, and R. C. Sun, Highly thermostable, flexible, and conductive films prepared from cellulose, graphite, and polypyrrole nanoparticles, *ACS Appl. Mater. Interfaces* 7(28), 15641 (2015)
44. L. Q. Zhang, S. G. Yang, L. Li, B. Yang, H. D. Huang, D. X. Yan, G. J. Zhong, L. Xu, and Z. M. Li, Ultralight cellulose porous composites with manipulated porous structure and carbon nanotube distribution for promising electromagnetic interference shielding, *ACS Appl. Mater. Interfaces* 11(2), 2559 (2019)
45. W. T. Cao, F. F. Chen, Y. J. Zhu, Y. G. Zhang, Y. Y. Jiang, M. G. Ma, and F. Chen, Binary strengthening and toughening of MXene/cellulose nanofiber composite paper with nacre-inspired structure and superior electromagnetic interference shielding properties, *ACS Nano*

12(5), 4583 (2018)
46. J. L. Hart, K. Hantanasirisakul, A. C. Lang, B. Anasori, D. Pinto, Y. Pivak, J. T. van Omme, S. J. May, Y. Gogotsi, and M. L. Taheri, Control of MXenes' electronic properties through termination and intercalation, *Nat. Commun.* 10(1), 522 (2019)
47. G. S. Lee, T. Yun, H. Kim, I. H. Kim, J. Choi, S. H. Lee, H. J. Lee, H. S. Hwang, J. G. Kim, D. W. Kim, H. M. Lee, C. M. Koo, and S. O. Kim, Mussel inspired highly aligned $Ti_3C_2T_x$ MXene film with synergistic enhancement of mechanical strength and ambient stability, *ACS Nano* 14(9), 11722 (2020)
48. M. Alhabeb, K. Maleski, B. Anasori, P. Lelyukh, L. Clark, S. Sin, and Y. Gogotsi, Guidelines for synthesis and processing of two-dimensional titanium carbide ($Ti_3C_2T_x$ MXene), *Chem. Mater.* 29(18), 7633 (2017)
49. B. Zhou, Z. Zhang, Y. L. Li, G. J. Han, Y. Z. Feng, B. Wang, D. B. Zhang, J. M. Ma, and C. T. Liu, Flexible, robust, and multifunctional electromagnetic interference shielding film with alternating cellulose nanofiber and MXene layers, *ACS Appl. Mater. Interfaces* 12(4), 4895 (2020)
50. W. Z. Bao, X. Tang, X. Guo, S. Choi, C. Y. Wang, Y. Gogotsi, and G. X. Wang, Porous cryo-dried MXene for efficient capacitive deionization, *Joule* 2(4), 778 (2018)
51. J. W. Fu, Z. H. Chen, M. H. Wang, S. J. Liu, J. H. Zhang, J. N. Zhang, R. P. Han, and Q. Xu, Adsorption of methylene blue by a high-efficiency adsorbent (polydopamine microspheres): Kinetics, isotherm, thermodynamics and mechanism analysis, *Chem. Eng. J.* 259, 53 (2015)
52. Y. Zhang, W. H. Cheng, W. X. Tian, J. Y. Lu, L. Song, K. M. Liew, B. B. Wang, and Y. Hu, Nacre-inspired tunable electromagnetic interference shielding sandwich films with superior mechanical and fire-resistant protective performance, *ACS Appl. Mater. Interfaces* 12(5), 6371 (2020)
53. Z. H. Zhou, Q. C. Song, B. X. Huang, S. Y. Feng, and C. H. Lu, Facile fabrication of densely packed Ti_3C_2 MXene/nanocellulose composite films for enhancing electromagnetic interference shielding and electro-/photothermal performance, *ACS Nano* 15(7), 12405 (2021)
54. X. F. Zhao, D. E. Holta, Z. Y. Tan, J. H. Oh, I. J. Echols, M. Anas, H. X. Cao, J. L. Lutkenhaus, M. Radovic, and M. J. Green, Annealed $Ti_3C_2T_z$ MXene films for oxidation-resistant functional coatings, *ACS Appl. Nano Mater.* 3(11), 10578 (2020)
55. Y. J. Wan, P. L. Zhu, S. H. Yu, R. Sun, C. P. Wong, and W. H. Liao, Anticorrosive, ultralight, and flexible carbon-wrapped metallic nanowire hybrid sponges for highly efficient electromagnetic interference shielding, *Small* 14(27), 1800534 (2018)
56. S. H. Ryu, Y. K. Han, S. J. Kwon, T. Kim, B. M. Jung, S. B. Lee, and B. Park, Absorption-dominant, low reflection EMI shielding materials with integrated metal mesh/TPU/CIP composite, *Chem. Eng. J.* 428, 131167 (2022)
57. L. Feng, Y. Zuo, X. He, X. J. Hou, Q. G. Fu, H. J. Li, and Q. Song, Development of light cellular carbon nanotube@graphene/carbon nanocomposites with effective mechanical and EMI shielding performance, *Carbon* 168, 719 (2020)
58. R. T. Liu, M. Miao, Y. H. Li, J. F. Zhang, S. M. Cao, and X. Feng, Ultrathin biomimetic polymeric $Ti_3C_2T_x$ MXene composite films for electromagnetic interference shielding, *ACS Appl. Mater. Interfaces* 10(51), 44787 (2018)
59. R. S. Li, L. Ding, Q. Gao, H. M. Zhang, D. Zeng, B. A. Zhao, B. B. Fan, and R. Zhang, Tuning of anisotropic electrical conductivity and enhancement of EMI shielding of polymer composite foam via CO_2-assisted delamination and orientation of MXene, *Chem. Eng. J.* 415, 128930 (2021)
60. Z. S. Liu, Y. Zhang, H. B. Zhang, Y. Dai, J. Liu, X. F. Li, and Z. Z. Yu, Electrically conductive aluminum ion-reinforced MXene films for efficient electromagnetic interference shielding, *J. Mater. Chem. C* 8(5), 1673 (2020)